Journal Name

Dynamic Article Links ►

Cite this: DOI: 10.1039/c0xx00000x

www.rsc.org/xxxxxx

ARTICLE TYPE

Double-degradable responsive self-assembled multivalent arrays – temporary nanoscale recognition between dendrons and DNA

Anna Barnard,[a] Paola Posocco,[b] Maurizio Fermeglia,[b] Ariane Tschiche,[c] Marcelo Calderon,[c] Sabrina Pricl,[b,d] and David K Smith*[a]

Received (in XXX, XXX) Xth XXXXXXXXX 20XX, Accepted Xth XXXXXXXXX 20XX

DOI: 10.1039/b000000x

This article reports self-assembling dendrons which bind DNA in a multivalent manner. The molecular design directly impacts on self-assembly which subsequently controls the way these multivalent nanostructures bind DNA – this can be simulated by multiscale modelling. Incorporation of an S-S linkage between the multivalent hydrophilic dendron and the hydrophobic units responsible for self-assembly allows these structures to undergo triggered reductive cleavage, with dithiothreitol (DTT) inducing controlled breakdown, enabling the release of bound DNA. As such, the high-affinity self-assembled multivalent binding is temporary. Furthermore, because the multivalent dendrons are constructed from esters, a second slow degradation step causes further breakdown of these structures. This two-step double-degradation mechanism converts a large self-assembling unit with high affinity for DNA into small units with no measurable binding affinity – demonstrating the advantage of self-assembled multivalency (SAMul) in achieving highly responsive nanoscale binding of biological targets.

Introduction

Multivalent interactions are a powerful strategic approach to achieve high-affinity interactions between objects on the nanometre length scale.[1] The organisation of multiple ligands to interact with multiple binding sites on a target, is therefore of vital importance in organising the nanoworld and developing new nanomaterials and nanomedicines.[2] However, one problem with multivalency is that the strong binding which results can often be relatively non-reversible and hence non-responsive.

In recent times, the concept of self-assembled multivalency (SAMul) has emerged – in this approach, multiple ligands are self-assembled to yield a nanoscale multivalent assembly.[3] The use of self-assembly endows these ligand arrays with simple synthesis,[4] gives a real degree of morphological control over the assembly,[5] and through co-assembly methods can easily generate multi-component multi-functional materials.[6] Furthermore, SAMul has a greater dynamic character than covalent multivalency, and provides the potential for such arrays to respond to stimulus.[7] In an elegant example, Scherman and co-workers used cucurbiturils in a self-assembled lectin-binding system, with binding being switched off by a simple chemical trigger (reduction of a viologen) which caused disassembly.[8]

Previously, we have investigated multivalent arrays of amine-derived ligands displayed on dendron surfaces and explored their ability to bind to DNA.[9] As a part of this work, we reported that degradation of the dendron framework can lead to structures which no longer bind to DNA – for example using UV-irradiation to cleave a photo-sensitive linker, leading to release of DNA.[10] Recently, however, rather than make high-generation dendrons, we have focussed on a SAMul approach, by designing small dendrons which can self-assemble into multivalent architectures. We, and others, have found that these systems, when self-assembled, can significantly outperform higher generation individual dendrons, illustrating the power of SAMul.[11] We have also demonstrated other advantages such as co-assembly with other units[12] and the ability to control the morphology[13] and biological activity of self-assembled nanostructures.[14]

To achieve temporary multivalency, we have incorporated degradability into the structure such that the units responsible for self-assembly become detached from the ligand groups. In this way, the self-assembling structure disassembles, and the multivalency is lost. We recently investigated the degradability of ester-derived SAMul dendrons for binding DNA, and showed that although the dendron on its own degraded and disassembled in a very efficient manner at pH 7.4, this degradation was promoted by intramolecular amine-catalysed ester hydrolysis, and was inactivated once the ligand array was bound to DNA.[15] As such, controlled loss of multivalency and release of DNA could not be achieved. In order to gain more controlled disassembly of our SAMul systems we therefore decided to incorporate disulfide linkages. Disulfides have previously been built into dendrons and their triggered reductive cleavage has been shown to lead to dendron degradation.[16] This approach is widely used to trigger the breakdown of synthetic gene delivery vectors,[17] but has not been quantified for triggering breakdown of a SAMul and hence inactivating binding. We intended to build this into a novel two-step degradation mechanism to switch off SAMul binding.

Cite this: DOI: 10.1039/c0xx00000x

www.rsc.org/xxxxxx

ARTICLE TYPE

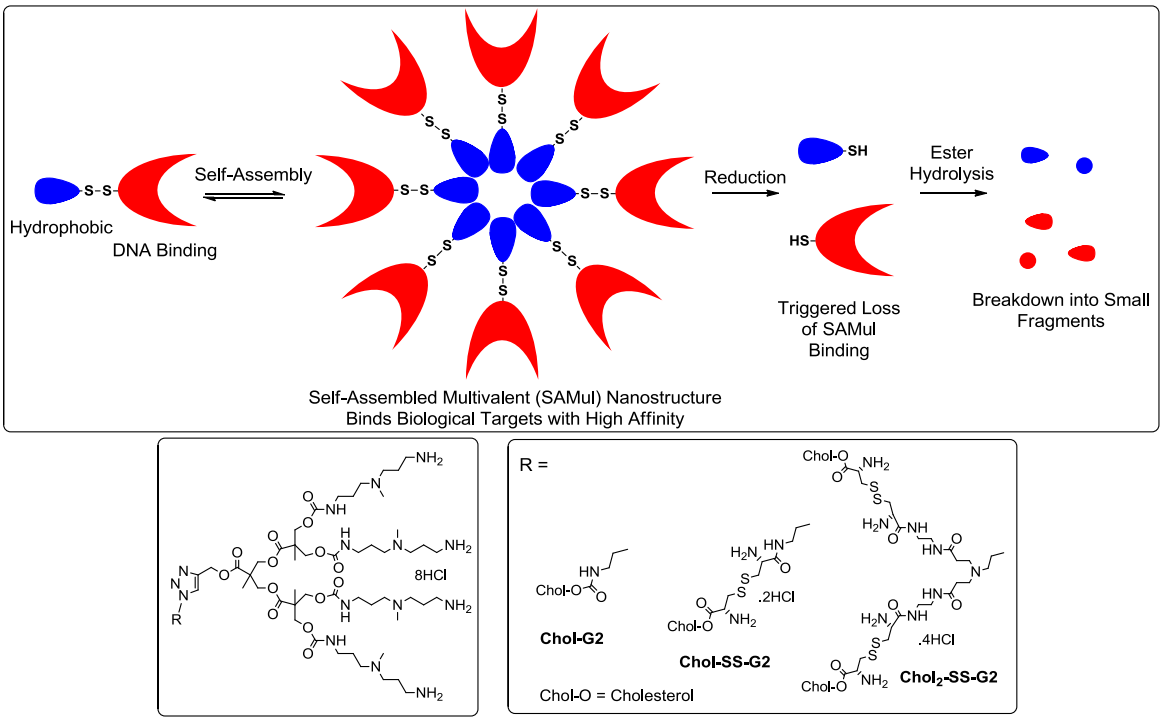

Fig. 1. Schematic of the concept of triggered loss of multivalent binding and dendron structures used in this work.

Dendron degradation has been quite widely exploited for the release of active units, such as drugs, from the termini of dendritic branches.[18] Furthermore, in key work, the degradation of self-assembled amphiphilic dendrimers has been achieved in a triggered manner using temperature, pH and enzymatic processes.[19] However, this approach has not previously been used in this manner to achieve the assembly and subsequent triggered dis-assembly of a multivalent binding interface capable of temporary intervention in biological processes.

Results and Discussion

Synthesis and Characterisation

To incorporate a disulfide linkage into our dendrons, we used a commercially available di-Boc protected dipeptide consisting of two cysteine amino acids joined by a disulfide bond. It was proposed to use this group to connect the hydrophobic unit, which drives the self-assembly process, with the ligand array responsible for DNA binding (Fig. 1). For the DNA-binding part of these compounds we used the Fréchet-Hult style ester dendrons,[20] modified with triamine ligands on their surfaces and an alkyne group at the focal point as previously reported.[15b] Two different hydrophobic units were used, one with a single cholesterol (**Chol**), and another with two cholesterols (**Chol$_2$**).

The synthesis of these dendrons is described in full in the supporting information, but is briefly outlined here. Cholesterol (**Chol**) was attached to di-Boc-cysteine using a DCC-mediated coupling reaction adapted from a procedure reported by Prokai *et al* for cholesterol modification[21] to give **Chol-SS-CO$_2$H**. This product was then subjected to a TBTU-mediated coupling with our previously reported azide-amine linker.[15b] This reaction proceeded in excellent yield affording azide-functionalised **Chol-SS-N$_3$**. The synthesis of the **Chol$_2$** unit was achieved by coupling previously reported azide-modified diamino PAMAM dendron[15] with **Chol-SS-CO$_2$H**. This was achieved via TBTU-mediated two-fold peptide coupling, and after purification by column chromatography, **Chol$_2$-SS-N$_3$** was isolated in a moderate yield.

The Boc-protected alkyne-functionalised dendron (**Alkyne-G2-Boc**) was coupled to the hydrophobic azides (**Chol-SS-N$_3$** or **Chol$_2$-SS-N$_3$**) via 'click' reactions. This was achieved in a 1:1 mixture of degassed THF and H_2O using $CuSO_4$ as catalyst and sodium ascorbate as reducing agent. Products were purified by size exclusion chromatography, yielding Boc-protected products which were then deprotected using HCl gas to produce the target compounds **Chol-SS-G2** and **Chol$_2$-SS-G2** in good yield and high purity. As a control, we decided to use our previously reported **Chol-G2**,[15b] which has similar hydrophobic and DNA binding units but does not have a degradable S-S linkage.

Self-Assembly Studies

With the target compounds in hand, we investigated their ability to self-assemble in water. Initially we probed this using a Nile Red uptake assay to estimate the critical micelle concentrations (CMCs, Table 1).[22] These CMC values clearly demonstrate that

the dendrons self-assemble in buffered water. Comparison of **Chol-SS-G2** with **Chol$_2$-SS-G2** indicates that the additional cholesterol unit significantly enhances self-assembly, with the CMC dropping from 13.3 μM to 5.2 μM. We argue that the increased hydrophobicity at the focal point improves the packing ability of the dendrons. It is noteworthy that **Chol-SS-G2** does not assemble as well as **Chol-G2**. We suggest that the linker, which itself has two protonatable amine groups on it, may hinder self-assembly to some extent due to the proximity of these hydrophilic groups to the hydrophobic cholesterol units.

Table 1. Compound charges (assuming all amines protonated), CMC values obtained from the Nile Red encapsulation assay, zeta potential and diameters (assuming spherical nanostructures) obtained from zeta-sizing.

Compound	Surface charge/ Total charge	CMC, μM	Zeta Potential, mV	Diameter, nm
Chol-G2	8+/8+	4.9 ± 0.6	+56.3 ± 4.4	6.32 ± 0.23
Chol-SS-G2	8+/10+	13.3 ± 1.6	+64.6 ± 1.5	10.7 ± 1.2
Chol$_2$-SS-G2	8+/12+	5.2 ± 0.4	+51.8 ± 7.1	10.7 ± 0.5

We employed zeta-sizing to provide insight into the size and surface charges of the assemblies which were being formed by these compounds (Table 1). The experimentally measured positive zeta potentials mean that all of these systems should be able to bind effectively to DNA. **Chol-SS-G2** and **Chol$_2$-SS-G2** both assembled into small spherical micelle-like aggregates of similar diameters (ca. 10.7 nm). This is slightly larger than the aggregates formed by **Chol-G2**, probably as a consequence of the extra space demands of the disulfide linker. Interestingly, although **Chol-SS-G2** and **Chol$_2$-SS-G2** have similar diameters, they have quite different zeta potentials. We suggest that this is because **Chol$_2$-SS-G2** forms assemblies containing fewer molecules – a consequence of the larger size of the di-cholesterol hydrophobic unit, which will take up more space within the interior of the aggregate leaving a less densely packed surface layer of protonated amines.

Table 2. Main characteristics of the spherical SAMul nanostructures as obtained from multiscale molecular simulations. N_{agg} = aggregation number; D_m = diameter; R_c = radius of hydrophobic densely packed core σ_m = surface charge per unit area; Ψ_s = surface electrostatic potential; ζ = zeta potential; ΔG_{mic} = free energy of micellisation; CMC = critical micellar concentration.

Compound	N_{agg}	D_m, nm	R_c, nm	σ_m, e/nm^2
Chol-G2	16 ± 1	3.9 ± 0.2	1.1 ± 0.1	2.7 ± 0.3
Chol-SS-G2	14 ± 3	5.8 ± 0.4	2.0 ± 0.2	1.3 ± 0.3
Chol$_2$-SS-G2	9 ± 1	5.2 ± 0.1	1.8 ± 0.1	1.3 ± 0.2
Compound	**Ψ_s, mV**	**ζ, mV**	**ΔG_{mic}, kcal/mol**	**CMC, μM**
Chol-G2	227.6	59.6	-23.0	0.035
Chol-SS-G2	182.6	52.8	-19.0	0.11
Chol$_2$-SS-G2	157.7	44.5	-20.2	0.039

To verify the hypotheses presented above we performed multiscale molecular simulations of the self-assembly processes of the modified dendrons. As shown in the left panel of Figure 2, both **Chol-SS-G2** and **Chol$_2$-SS-G2** are predicted to self-assemble into spherical micelles, having the characteristics listed in Table 2. Pleasingly, the calculated micellar diameters for **Chol-SS-G2** and **Chol$_2$-SS-G2** are sensibly larger (5.8 and 5.2 nm, respectively) than the diameter estimated for **Chol-G2** (3.9 nm), notwithstanding their lower aggregation number N_{agg} (Table 2). This is due to the steric hindrance and Coulombic repulsion being exerted by the relatively large charged linker in the new derivatives, which hampers the efficient molecular packing of the micellar core, ultimately resulting in larger assemblies. Of note, the micellar aggregate dimensions estimated *in silico* nicely correlate with the hydrodynamic diameters measured by DLS (6.3-10.7 nm), since the experimental value also includes the hydrodynamic water shell which, by definition, is larger than the pure amphiphile (3-6 nm).

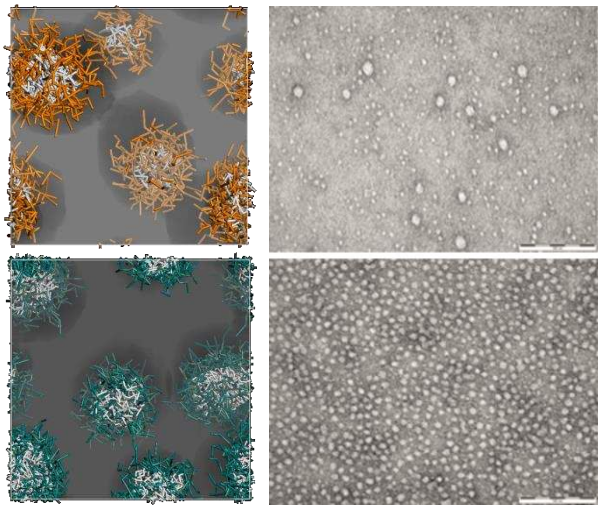

Fig. 2. (Left) Micellar structures of **Chol-SS-G2** (top) and **Chol$_2$-SS-G2** (bottom) as predicted from mesoscopic simulations. The hydrophobic core is in white sticks while the hydrophilic head is in orange and dark cyan, respectively. (Right) TEM images of dried aqueous samples of **Chol-SS-G2** (top) and **Chol$_2$-SS-G2** (bottom) illustrating spherical micellar self-assemblies. Scale bar = 100 nm.

Clearly the presence of the linker seems to significantly increase the diameter of the self-assembled nanostructures – more than might be expected just based on the extra spacing effect. In order to probe the reasons for this, we used multiscale modelling to determine the density distribution of matter within the micellar cores. As can be seen in Figure 3 and Table 2, the core of the micelle formed by **Chol-G2** is more compact and the density is higher (radius = R_c, depicted by red area). Conversely, the nanostructures formed by **Chol-SS-G2** and **Chol$_2$-SS-G2** have less dense, more loosely packed micellar cores (smaller high density red areas, changing to lower density blue). This is a consequence of repulsion between the charged linkers and the overall higher steric hindrance.

The simulated CMC values show that, with respect to **Chol-G2**, the presence of a larger, charged linker in **Chol-SS-G2** decreases the packing efficiency of the cores of the nanostructures formed by these dendrons and, increases the CMC – supporting the analysis in Fig. 3. On the other hand, adding a further cholesterol unit at the dendron focal point is beneficial, with the additional hydrophobic interactions outweighing the steric and electrostatic repulsions induced by the linker – as such, the CMC is lower, similar to that found for **Chol-G2**. Although the absolute values of these simulated CMCs should be treated with caution, the trends are clearly in agreement with the experimental data.

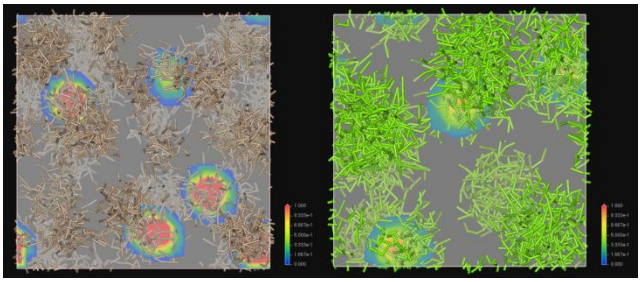

Fig. 3. Mesoscale density distribution inside the core of micelles of **Chol-G2** (left) and **Chol-SS-G2** (right). High density areas are shown in red, and lower density areas in green and blue. The dendrons are portrayed as beige and green sticks respectively. A transparent grey field is used to represent water and ions. Images are not in scale with each other.

Calculated values of zeta potential, ζ, are rarely obtained using this kind of modelling approach and provide an important insight. They can be rationalized on the basis of the micellar characteristics discussed above. As the surface electrostatic potential of the micelles, Ψ_s, is proportional to the micelle surface charge per unit area (σ_m, Table 2), Ψ_s increases with increasing N_{agg} and decreasing micellar dimensions, hence leading to the final ζ values shown in Table 2. Accordingly, **Chol-G2** has the highest σ_m and ζ values, followed by **Chol-SS-G2** and **Chol$_2$-SS-G2**. This is slightly different to our experimental observations, where **Chol-SS-G2** had a higher zeta potential than **Chol-G2**, this may reflect problems associated with the charges on the linker group in **Chol-SS-G2**, which may, or may not, be located on the surface of the final self-assembled nanostructures, and the fact that this system, perhaps as a result, assembles into more polydisperse nanostructures (*vide infra*). Our *in silico* calculations of ζ support the notion that all systems should be able to bind DNA, although to different extents.

In order to observe the morphology of self-assembly experimentally, we employed transmission electron microscopy (TEM) methods to visualise the nanostructures being formed. The compounds were dissolved in water at a concentration of 1 mM, well above their CMC, and dried on the TEM grid. The TEM images (Figure 2) and provide supporting evidence that the dendrons assemble in aqueous solution into spherical micellar-type assemblies. The aggregates formed by **Chol-SS-G2** and **Chol$_2$-SS-G2** have diameters of approximately 10 nm, in agreement with the solution phase DLS data. Notably, although the assemblies formed from **Chol$_2$-SS-G2** were remarkably monodisperse, showing very little variation in diameter, those formed by **Chol-SS-G2** had a broader range of sizes. This is in agreement with the errors observed from DLS measurements. Interestingly, both qualitative (Fig. 2, left) and quantitative analyses (D_m, Table 2) of the mesoscopic simulations of these systems also suggested a more polydisperse character of the **Chol-SS-G2** micelles, while an almost uniform distribution of aggregates was found for the other systems. This suggests that the aggregates formed from the more hydrophobic system (**Chol$_2$-SS-G2**) are more stable and, as a consequence, much better structurally defined. This might be expected on the basis of them having a greater cohesive energy as a consequence of the larger hydrophobic surfaces driving self-assembly, whereas for **Chol-SS-G2**, the cohesive energy provided by hydrophobic interactions is less able to overcome the electrostatic repulsions between protonated amine groups, particularly those which are not on the surface, but instead on the linker unit.

DNA Binding Studies

We then investigated the ability of these SAMul nanostructures to bind DNA using ethidium bromide (EthBr) displacement assays from calf thymus DNA,[23] and gel electrophoresis to monitor binding to pGL3 plasmid DNA (Table 3). For the purposes of these data, and for fair comparison, we assumed that only the surface charges of the dendrons were responsible for DNA binding, and that those on the linker do not play an active role. It should also be noted that N:P ratios determined from electrophoresis measure the complete retardation of the DNA rather than 50% binding/displacement and, so, are generally higher than the values obtained in the EthBr assay. Importantly, in the absence of any hydrophobic modification, the G2 dendron is incapable of effective DNA binding (data not shown) – and as such, SAMul plays a key role in all of the binding discussed.

Table 3. Compound surface charge (assuming only the surface amines provide primary interaction with DNA), CE_{50} values obtained from the EthBr displacement assay with calf thymus DNA, and N:P ratio required to fully retard pGL3 plasmid DNA in a gel electrophoresis well.

Compound	Surface Charge	CE_{50} (EthBr Displacement)	N:P (Gel Electrophoresis)
Chol-G2	8+	0.66 ± 0.13	2.09
Chol-SS-G2	8+	0.91 ± 0.06	1.54
Chol$_2$-SS-G2	8+	1.05 ± 0.07	2.17

For the disulfide-linked G2 dendrons, the system with less hydrophobic modification is a more effective DNA binder – this is in agreement with the experimental and simulated zeta potential results (Tables 1 and 2) which indicated that the hydrophobic/hydrophilic balance of **Chol-SS-G2** is such that it has a higher surface charge density than **Chol$_2$-SS-G2**. However, it should also be noted that **Chol-G2** is better than the degradable dendrons in the EthBr assay, and comparable to the best in gel electrophoresis. We suggest that for the degradable dendrons, in contrast to **Chol-G2**, the amine groups present on the disulfide linker – distant from the surface of the self-assembled nanostructures – may somewhat hinder effective self-assembly and DNA binding – in agreement with the observations of looser self-assembly for these disulfide-linked systems (Fig. 3).

Additional molecular simulations were performed at this point to rank the affinity of each SAMul micelle/DNA system. As shown in Table 4, the micelles formed by **Chol-G2** are characterized by a total charge of +128, 40 of which are effectively involved in contacting the DNA fragment. Conversely, the SAMul nanocarriers generated by **Chol-SS-G2** and **Chol$_2$-SS-G2** are able to exploit only 36 and 21 (out of their total 112 and 72 surface positive charges, respectively), to constantly bind DNA (Fig. 4). In order to compare these data with the CE_{50} values, we took the overall ΔG_{bind}, and divided it by the total available surface charge. In agreement with the experimental data, the theoretical study supports the ranking of the affinity of our SAMul systems towards short DNA fragments in the order: **Chol-G2 > Chol-SS-G2 > Chol$_2$-SS-G2**.

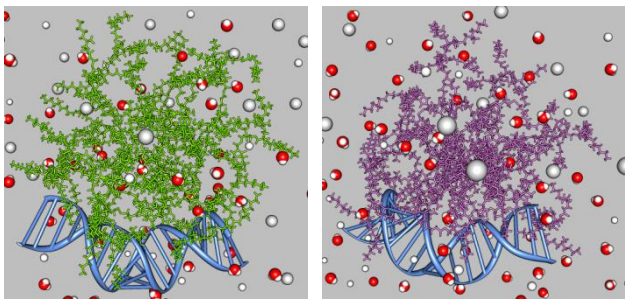

Fig. 4. Molecular dynamics simulation snapshots of **Chol-SS-G2** (left) and **Chol$_2$-SS-G2** (right) complexed with a 21 bp DNA fragment. The modified dendrons are portrayed as green and purple sticks, while the DNA duplex is shown in a stair-ribbon representation. Some water molecules are visualized as CPK spheres (O, red; H, white), while some Na^+ and Cl^- counterions are shown as small and large grey-shaded spheres, respectively.

Table 4. Free energy of binding (ΔG_{bind}), number of surface charges and surface-charge-normalized free energy of binding (ΔG_{bind}/Charge) for DNA/SAMul nanocarrier complexes as derived from molecular simulations.

Compound	ΔG_{bind}, kcal/mol	Surface Charge	ΔG_{bind}/Charge, kcal/mol
Chol-G2	-82.1 ± 2.2	+128	-0.64 ± 0.02
Chol-SS-G2	-58.8 ± 1.6	+112	-0.53 ± 0.02
Chol$_2$-SS-G2	-17.9 ± 1.3	+72	-0.25 ± 0.02

We also calculated the affinity of only those surface charges which formed stable contacts with DNA (Table 5). This was done by calculating the binding energy associated only with these contacts ($\Delta G_{bind,eff}$), and dividing by the number of these stable contacts (N_{eff}) to give the affinity of each stable contact ($\Delta G_{bind,eff}/N_{eff}$). This demonstrates that the value of each stable contact is greater for **Chol-G2** and that **Chol-SS-G2** is better able to use its individual charges to bind DNA than **Chol$_2$-SS-G2**.

Table 5. Free energy of binding associated with effective stable contacts ($\Delta G_{bind,eff}$), number of stable binding contacts on nanostructure surface (N_{eff}) and effective contact-normalized free energy of binding ($\Delta G_{bind,eff}/N_{eff}$) for DNA/SAMul nanocarrier complexes as derived from molecular simulations.

Compound	$\Delta G_{bind,eff}$ kcal/mol	N_{eff}	$\Delta G_{bind,eff}/N_{eff}$, kcal/mol
Chol-G2	-34.7 ± 0.7	40 ± 1	-0.87 ± 0.03
Chol-SS-G2	-18.4 ± 0.5	36 ± 2	-0.51 ± 0.03
Chol$_2$-SS-G2	-4.83 ± 0.3	21 ± 1	-0.23 ± 0.02

To probe DNA binding in more detail, zeta potential measurements were carried out in the presence of a 21 base-pair repeat of DNA (Table 6). Although each of the dendrons was able to condense DNA, it was notable that in agreement with all the other methods of study, **Chol-G2** was best able to neutralise the charge, and gave rise to small (ca. 100-150 nm) assemblies at a relatively low N:P value of 2. Notably, **Chol-SS-G2** was better able to condense the DNA at the N:P ratio of 5 than **Chol$_2$-SS-G2**, in agreement with our observation that the system with only one hydrophobic cholesterol group was the more effective DNA binder, possibly as a consequence of its higher zeta potential.

It should be noted that the model depicted in Figure 3 may appear to suggest 1:1 stochiometry – which is not consistent with the sizes of the complexes observed by DLS (Table 6). Obviously, the model in Figure 4 is a necessary simplification. As indicated by mesoscale modelling (Fig. 5) DNA polymer chains can interact with multiple self-assembled multivalent nanostructures (and vice versa). This leads to clustering of the nanostructures and gives rise to the larger nanoscale objects reported in Table 6.

Table 6. - Zeta potential and average aggregate diameters determined by zeta sizing and DLS measurements (volume distribution) in the presence of 21 base-pair repeat DNA at different N:P ratios (these N;P ratios take account of all the amines, not only those on the dendron surface). PDI represents the polydispersity of these aggregates.

Compound	N:P	Zeta, mV	Diameter, nm	PDI
DNA		-49.8 ± 1.8		
Chol-G2		+56.3 ± 4.4	6.32 ± 0.23	0.360
	1	+8.0 ± 3.1	333.2 ± 20.2	0.177
	2	+26.0 ± 2.6	126.3 ± 0.8	0.164
	5	+48.8 ± 1.1	106.6 ± 0.4	0.168
	10	+51.3 ± 2.0	143.9 ±0.5	0.163
Chol-SS-G2		+64.6 ± 1.5	10.7 ± 1.2	0.714
	1	-41.4 ± 1.4	217.8 ± 16.4	0.411
	2	-4.3 ± 0.6	688.3 ± 76.6	0.198
	5	+33.6 ± 4.6	112.8 ± 31	0.376
	10	+46.0 ± 0.9	102.3 ± 15.4	0.755
Chol$_2$-SS-G2		+51.8 ± 7.1	10.7 ± 0.5	0.980
	1	-9.5 ± 0.5	583.9 ± 88.7	0.101
	2	+14.6 ± 0.5	346.1 ± 45.8	0.149
	5	+37.3 ± 2.9	173.0 ± 2.0	0.108
	10	+45.5 ± 3.0	88.1 ± 2.4	0.199

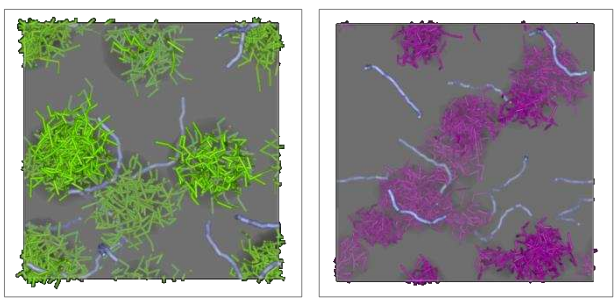

Fig. 5. Mesoscale modelling of **Chol-SS-G2** (left) and **Chol$_2$-SS-G2** (right) complexed with a 21 bp DNA fragment. The dendrons are portrayed as purple and green sticks respectively, while the DNA molecule is depicted as a light blue stick. A transparent grey field is used to represent water and ions.

Triggered Degradation, Disassembly and Loss of Self-Assembled Multivalency

To determine if triggered degradation leads to dissociation of the hydrophobic groups, and subsequent dis-assembly, a Nile Red encapsulation study was performed.[22] A solution of each dendron was prepared in PBS buffer at concentrations well above their CACs: 200 μM for **Chol-SS-G2** and 20 μM for **Chol$_2$-SS-G2**. Nile Red was then added and its fluorescence was determined as it resided in the hydrophobic interior of the self-assembled nanostructure. At time zero, dithiothreitol (DTT) was added to give a reducing agent concentration of 10 mM. The fluorescence intensity was recorded over a period of 30 minutes. Any decrease in fluorescence was considered to be characteristic of the loss of a self-assembled hydrophobic environment able to encapsulate Nile Red. The data (Fig. 6) show that 10 mM DTT leads to rapid (<5

min) cleavage of the disulfide bond at the focal point of both of the reducible dendrons which, in turn, leads to disassembly and release of Nile Red. Conversely, **Chol-G2** (for data, see SI) remained unaffected by the addition of DTT, indicating that self-assembled nanostructures without a disulfide linkage remain fully stable. The system with two cholesterol groups appears to be broken down more rapidly, but it should be noted that the two systems were investigated at different concentrations, and furthermore, once one of the cholesterol groups has been removed from **Chol$_2$-SS-G2** the CMC value will significantly change. In any case, this result highlights the potential of these compounds to act as responsive SAMul DNA binders.

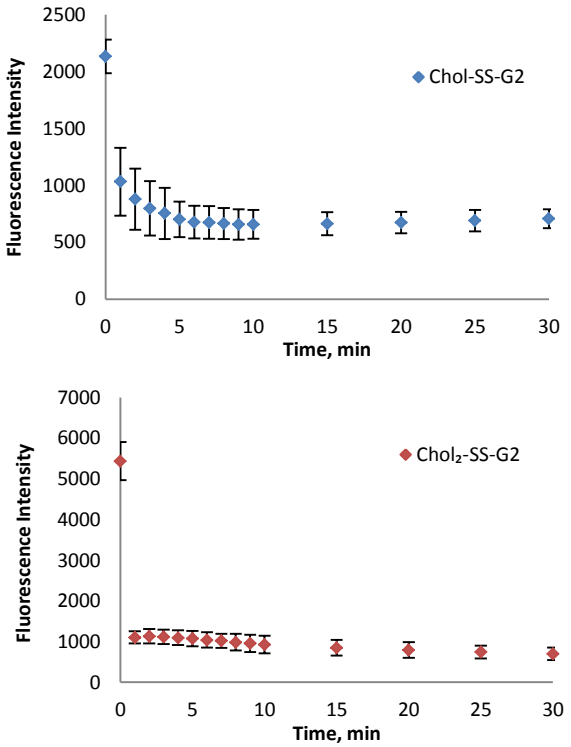

Fig. 6. Fluorescence intensity (635 nm) of Nile Red in the presence of **Chol-SS-G2** (top, 200 μM) and **Chol$_2$-SS-G2** (bottom, 20 μM) over time in the presence of 10 mM DTT showing degradation and disassembly leading to release of Nile Red from the hydrophobic micelle interior.

Disassembly and Loss of Multivalent Binding

To determine if degradation and disassembly can therefore be used to switch off multivalent interactions with DNA, we employed an ethidium bromide (EthBr) assay. The dendron was added to DNA/EthBr at an N:P ratio of 2, binding to the DNA and hence lowering EthBr fluorescence. If subsequent dendron degradation leads to loss of SAMul binding, then DNA will be released and EthBr will be able to re-intercalate into the DNA double helix and the fluorescence of EthBr will be switched on.[15]

Initially, we monitored dendron stability in the absence of DTT to determine whether ester degradation was able to induce disassembly and DNA release. After stirring for 5 days at 37°C there was no evidence of any DNA decomplexation for **Chol-G2** or **Chol-SS-G2** (data in SI), supportive of our previous work showing that ester degradation is shut-down in this system by DNA binding, which inhibits intramolecular amine-catalysed ester hydrolysis.[15b] There is however, some indication that DNA release does occur initially for **Chol$_2$-SS-G2** (Fig. 7). Over 24 hours, some DNA was released but was then re-complexed as the timescale increases. From MS data (*vide infra*), we have some evidence for disulfide bond cleavage even in the absence of reducing agent and we suggest that in this case, these bonds equilibrate leading to slow re-arrangement of DNA binding.

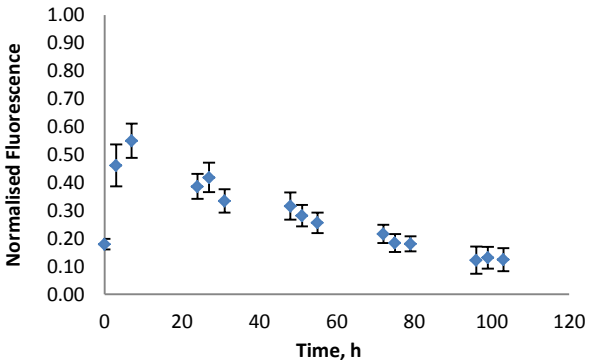

Fig. 5. Fluorescence data for **Chol$_2$-SS-G2** (bottom) stirred at 37 °C in the presence of calf thymus DNA (N:P = 2) and ethidium bromide showing some initial DNA release and subsequent rebinding.

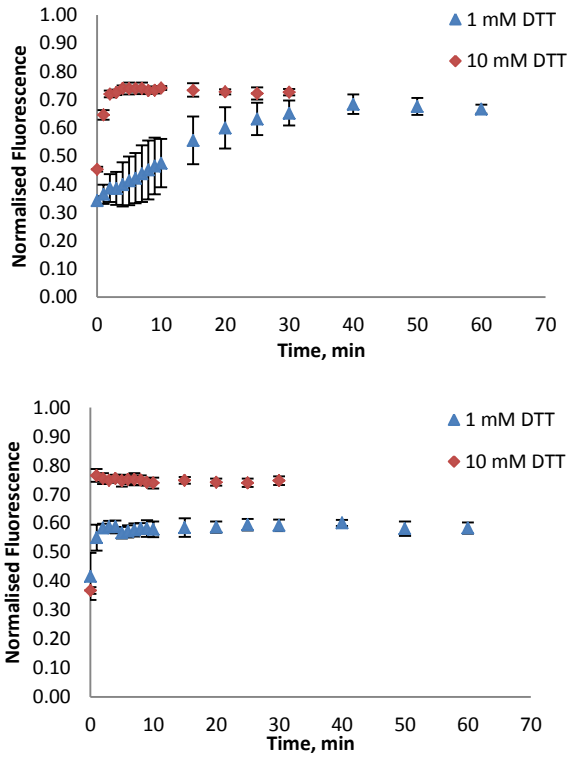

Fig. 7. Fluorescence data for **Chol-SS-G2** (top) and **Chol$_2$-SS-G2** (bottom) stirred at 37 °C in the presence of calf thymus DNA (N:P = 2), ethidium bromide and either 1 or 10 mM DTT.

We then probed the effect of DTT on DNA binding affinity. The EthBr DNA release experiment was repeated in the presence of both 1 and 10 mM DTT (Fig. 8). It should be noted that the timescale for these experiments was minutes, rather than the hours used in the absence of DTT. Pleasingly, this assay shows quite clearly that the addition of a reducing agent leads to very rapid triggered release of bound DNA due to cleavage of the internal disulfide bonds in the dendrons. Furthermore, the kinetics

of DNA release are dependent on the concentration of DTT, demonstrating that this reagent is driving degradation.

Both **Chol-SS-G2** and **Chol$_2$-SS-G2** released DNA in the presence of 1 mM DTT in less than one hour. At higher concentrations of reducing agent (10 mM) the release occurred even more rapidly (<5 min). It is also evident that **Chol$_2$-SS-G2** was able to liberate DNA at a faster rate than **Chol-SS-G2**. This is possibly a result of the presence of the additional disulfide bond in the di-cholesterol-functionalised compound. This result agrees with the previous observations from the Nile Red assay, although in this assay, unlike the previous one, both dendrons are present at very similar concentration, suggests that there is indeed an innate difference in the rate of triggered degradation, with **Chol$_2$-SS-G2** being more effectively broken down.

We next monitored the stability of the dendrons by mass spectrometry in ammonium bicarbonate buffer (10 mM) using methods previously reported by us.[15b] We reasoned that this would allow us to probe the two different pathways by which degradation can occur (triggered disulfide breakdown or slow ester cleavage) in more detail.

The samples were analysed by mass spectrometry at the beginning of the assay and after 24 hours stirring at 37°C. A second sample was then prepared at the same concentration and dithiothreitol (DTT) was added at a concentration of 10 mM. This solution was also analysed by mass spectrometry after 24 hours. Obviously, it should be noted that in such an assay, the presence or absence of peaks, and their absolute heights cannot be used to precisely detect or quantify what is present, as different degraded fragments have different detection sensitivities. Nonetheless, it can provide some insight into the degradation pathways taking place, and relative intensities can be used to monitor changes in relative product distributions. For full details of all mass spectra and peak assignments, see the supporting information.

We have previously reported that for **Chol-G2** the ester scaffold slowly degrades over a period of ca. 12 hours. As such, we expected all of these dendrons to exhibit slow degradation of the ester units – this was indeed the case. The kinetics of this background ester degradation are much slower than the DTT-induced disulfide breakdown as monitored above. Perhaps surprisingly, however, in the presence of DTT, there was no MS evidence for the cleavage of the disulfide bond in **Chol-SS-G2**, although the aggregation and binding assays described above clearly indicate that this is taking place. We suggest that the peaks corresponding to the degradation products are not visible by MS under these experimental conditions or that further degradation of the fragments makes them impossible to observe.

For the compound bearing two cholesterol groups at the focal point, **Chol$_2$-SS-G2**, in addition to the slow ester bond cleavage, we also saw clear evidence for the cleavage of disulfide bonds. Interestingly, we also observed some thiol products in the spectra even in the absence of DTT, suggesting that the disulfide bonds may be cleaved in aqueous solution. This cannot be an artefact of MS ionisation, as these peaks were absent in the starting spectrum. This agrees with the changes in DNA binding on incubation of **Chol$_2$-SS-G2** in buffer described above (Fig. 7). Importantly though, the reducing agent (DTT) significantly increased the relative intensity of the peaks (versus calibrant) corresponding to disulfide cleavage products of **Chol$_2$-SS-G2** (Fig. 9), suggesting that DTT leads to triggered enhancement of reductive degradation. In addition, the peaks associated with ester degradation products decreased in relative intensity (Fig. 9), presumably as the disulfide degradation pathway became dominant. It is therefore clear that for **Chol$_2$-SS-G2** both degradation pathways operate, but that DTT triggers a greater relative degree of rapid degradation via reductive cleavage. It was therefore clear from these MS studies that over a 24 hour timescale, all three dendrons degrade via ester hydrolysis and that for **Chol$_2$-SS-G2** disulfide degradation, enhanced by DTT could also be detected.

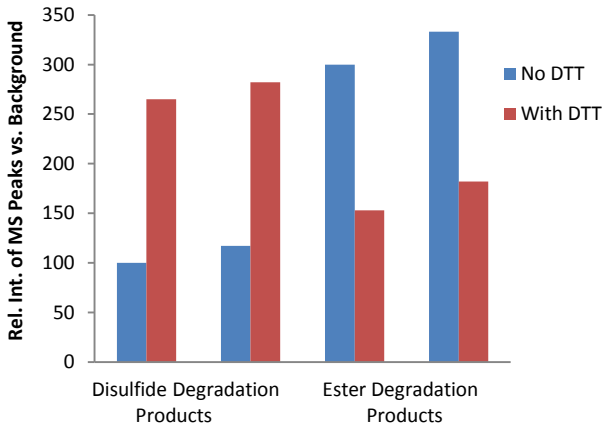

Fig. 9. Addition of DTT enhances the relative intensity of MS peaks associated with disulfide reduction products (versus background calibrant).

In combination, these assays demonstrate that rapid disulfide cleavage in the presence of DTT leads to triggered disassembly and loss of SAMul binding of DNA. The products, which have released their grip on DNA, are then able to slowly degrade further into smaller fragments through an ester hydrolysis mechanism, which does not operate if DNA is still bound to the dendrons.[15b] As such, these dendrons have double-degradable frameworks, clearly illustrating how SAMul can respond to different chemical triggers in a controllable way.

Conclusions

In summary, we have reported novel disulfide-linked dendrons which self-assemble into nanostructures and bind DNA through the resulting multivalent interactions. The degree of hydrophobic modification controls the size and charge density of the nanostructures, and this has a direct impact on the DNA binding ability. These effects are supported by multiscale modelling methods. The addition of DTT as a reducing agent leads to triggered reductive cleavage of the disulfide linkage, which disconnects the hydrophobic unit from the DNA binding fragment, and consequently leads to disassembly and loss of self-assembled multivalent binding. After decomplexation of DNA, the ester-linkages in these dendrons will also undergo slow degradation over longer timescales leading to further fragmentation of the multivalent self-assembling system into small units. We have therefore clearly demonstrated how SAMul binding can easily be manipulated and controlled in a two-step

double-degradation process, such that high-affinity binding can be expressed in a temporary manner. This binding strategy is of relevance in nanomedicine and we are currently exploiting these methods to bind a variety of different biological targets in a transient and controllable manner.

Acknowledgements

We thank BBSRC (DTA award) for funding and COST Network TD0802 (Dendrimers in Biomedicine) for supporting networking within this project. Access to CINECA and supercomputing facility was granted through the sponsored HPC Italian Supercomputing Resource Allocation (ISCRA) projects MONALISA, NANO4HEALTH and SEA.

Notes and references

[a] *Department of Chemistry, University of York, Heslington, York, YO10 5DD. Fax:+44 (0)1904 324516; E-mail: david.smith@york.ac.uk*

[b] *National Interuniversity Consortium for Material Science and Technology (INSTM), Research Unit MOSE-DEA, University of Trieste, 34127 Trieste, Italy.*

[c] *Institut für Chemie und Biochemie, Freie Universität Berlin, Takustrasse 3, D-14195 Berlin, Germany.*

[d] *Molecular Simulation Engineering (MOSE) Laboratory, Department of Engineering and Architecture (DEA), University of Trieste, 34127 Trieste, Italy*

† Electronic Supplementary Information (ESI) available: full synthetic methodology and characterisation data for novel dendrons, original data from self-assembly and DNA binding assays, mass spectrometric data, further data from degradation assays and details of multiscale modeling methods. See DOI: 10.1039/b000000x/

1 (*a*) M. Mammen, S. K. Choi and G. M. Whitesides, *Angew. Chem.-Int. Edit.* 1998, **37**, 2755-2794. (*b*) S. E. Stiriba, H. Frey and R. Haag, *Angew. Chem. Int. Ed.* 2002, **41**, 1329-1334. (*c*) A. Mulder, J. Huskens and D. N. Reinhoudt, *Org. Biomol. Chem.* 2004, **2**, 3409-3424. (*d*) J. D. Badjic, A. Nelson, S. J. Cantrill, W. B. Turnbull and J. F. Stoddart, *Acc. Chem. Res.* 2005, **38**, 723-732. (*e*) V. Martos, P. Castreño, J. Valero and J. de Mendoza, *Curr. Opin. Chem. Biol.* 2008, **12**, 698-706. (*f*) G. M. Pavan, A. Danani, S. Pricl and D. K. Smith, *J. Am. Chem. Soc.* 2009, **131**, 9686-9694.

2 C. Fasting, C.A. Schalley, M. Weber, O. Seitz, S. Hecht, B. Koksch, J. Dernedde, C. Graf, E.W. Knapp and R. Haag, *Angew. Chem. Int. Ed.* 2012, **51**, 10472-10498.

3 (*a*) A. Barnard and D. K. Smith, *Angew. Chem. Int. Ed.* 2012, **51**, 6572-6581. (*b*) K. Petkau-Milroy and L. Brunsveld, *Org. Biomol. Chem.* 2013, **11**, 219-232. (*c*) P. M. Levine, T. P. Carberry, J. M. Holub and K. Kirshenbaum, *Med. Chem. Commun.* 2013, **4**, 493-509.

4 (*a*) J. E. Kingerywood, K. W. Williams, G. B. Sigal and G. M. Whitesides, *J. Am. Chem. Soc.* 1992, **114**, 7303-7305. (*b*) J. D. Hartgerink, E. Beniash and S. I. Stupp, *Science* 2001, **294**, 1684-1688. (*c*) G. Thoma, A. G. Katopodis, N. Voelcker, R. O. Duthaler and M. B. Streiff, *Angew. Chem. Int. Ed.* 2002, **41**, 3195-3198. (*d*) G. A. Silva, C. Czeisler, K. L. Niece, E. Beniash, D. A. Harrington, J. A. Kessler and S. I. Stupp, *Science* 2004, **303**, 1352-1355. (*e*) M. K. Muller and L. Brunsveld, *Angew. Chem. Int. Ed.* 2009, **48**, 2921-2924. (*f*) D. J. Welsh and D. K. Smith, *Org. Biomol. Chem.* 2011, **9**, 4795-4801.

5 (*a*) B. S. Kim, D. J. Hong, J. Bae and M. Lee, *J. Am. Chem. Soc.* 2005, **127**, 16333-16337. (*b*) D.-W. Lee, T. Kim, I.-S. Park, Z. Huang and M. Lee, *J. Am. Chem. Soc.* 2012, **134**, 14722-14725.

6 (*a*) M. R. Dreher, A. J. Simnick, K. Fischer, R. J. Smith, A. Patel, M. Schmidt and A. Chilkoti, *J. Am. Chem. Soc.* 2008, **130**, 687-694. (*b*) A. J. Simnick, C. A. Valencia, R. H. Liu and A. Chilkoti, *ACS Nano* 2010, **4**, 2217-2227. (*c*) K. Petkau, A. Kaeser, I. Fischer, L. Brunsveld and A. P. H. J. Schenning, *J. Am. Chem. Soc.* 2011, **133**, 17063-17071. (*d*) Y. Lim, S. Park, E. Lee, J.-H. Ryu, Y.-R. Yoon, T.-H. Kim and M. Lee, *Chem. Asian J.* 2007, **2**, 1363-1369. (*e*) H. Storrie, M. O. Guler, S. N. Abu-Amara, T. Volberg, M. Rao, B. Geiger and S. I. Stupp, *Biomaterials* 2007, **28**, 4608-4618.

7 (*a*) J.-H. Ryu, E. Lee, Y.-B. Lim and M. Lee, *J. Am. Chem. Soc.* 2007, **129**, 4808-4814. (*b*) D. Jiao, J. Geng, X. J. Loh, D. Das, T.-C. Lee and O. A. Scherman, *Angew. Chem. Int. Ed.* 2012, **51**, 9633-9637.

8 J. Geng, F. Biedermann, J. M. Zayed, F. Tian and O. A. Scherman, *Macromolecules* 2011, **44**, 4276-4281.

9 (*a*) M. A. Kostiainen, J. G. Hardy and D. K. Smith, *Angew. Chem. Int. Ed.* 2005, **44**, 2556-2559. (*b*) G. M. Pavan, A. Danani, S. Pricl and D. K. Smith, *J. Am. Chem. Soc.* 2009, **131**, 9686-9694. (*c*) S. P. Jones, G. M. Pavan, A. Danani, S. Pricl and D. K. Smith, *Chem. Eur. J.* 2010, **16**, 4519-4532.

10 (*a*) M. A. Kostiainen, D. K. Smith and O. Ikkala, *Angew. Chem. Int. Ed.* 2007, **46**, 7600-7604. (*b*) G. M. Pavan, M. A. Kostiainen and A. Danani, *J. Phys. Chem. B* 2010, **114**, 5686-5693. (*c*) M. A. Kostiainen, J. Kotimaa, M. L. Laukkanen and G. M. Pavan, *Chem. Eur. J.* 2010, **16**, 6912-6918. (*d*) M. A. Kostiainen, O. Kasyutich, J. J. L. M. Cornelissen and R. J. M. Nolte, *Nature Chem.* 2010, **2**, 394-399. (*e*) W. Fischer, M. A. Quadir, A. Barnard, D. K. Smith and R. Haag, *Maromol. Biosci.* 2011, **11**, 1736-1746.

11 (*a*) P. Posocco, S. Pricl, S. Jones, A. Barnard and D. K. Smith, *Chem. Sci.* 2010, **1**, 393-404. (*b*) S. P. Jones, N. P. Gabrielson, C.-H. Wong, H.-F. Chow, D. W. Pack, M. Fermeglia, S. Pricl and D. K. Smith, *Mol. Pharm.* 2011, **8**, 416-429. (*c*) T. Z. Yu, X. X. Liu, A. L. Bolcato-Bellemin, Y. Wang, C. Liu, P. Erbacher, F. Qu, P. Rocchi, J.-P. Behr and L. Peng, *Angew. Chem. Int. Ed.* 2012, **51**, 8478-8484. (*d*) D. Joester, M. Losson, R. Pugin, H. Heinzelmann, E. Walter, H. P. Merkle and F. Diederich, *Angew. Chem. Int. Ed.* 2003, **42**, 1486-1490. (*e*) M. Guillot, S. Eisler, K. Weller, H. P. Merkle, J. L. Gallani and F. Diederich, *Org. Biomol. Chem.* 2006, **4**, 766-769. (*f*) H. K. Bayele, T. Sakthivel, M. O'Donell, K. J. Pasi, A. F. Wilderspin, C. A. Lee, I. Toth and A. T. Florence, *J. Pharm. Sci.* 2005, **94**, 446-457. (*g*) H. K. Bayele, C. Ramaswamy, A. F. Wilderspin, K. S. Srai, I. Toth and A. T. Florence, *J. Pharm. Sci.* 2006, **95**, 1227-1237. (*h*) K. C. Wood, S. R. Little, R. Langer and P. T. Hammond, *Angew. Chem. Int. Ed.* 2005, **44**, 6704-6708. (*i*) K. C. Wood, S. M. Azarin, W. Arap, R. Pasqualini, R. Langer and P. T. Hammond, *Bioconjugate Chem.* 2008, **19**, 403-405. (*j*) Z. Poon, J. A. Lee, S. Huang, R. J. Prevost and P. T. Hammond, *Nanomedicine* 2011, **7**, 201-209.

12 A. Barnard, A. Tschiche, M. Calderon, R. Haag and D. K. Smith, *Org Biomol Chem*, 2012, **10**, 8403-8409.

13 D. J. Welsh, P. Posocco, S. Pricl and D. K. Smith, *Org. Biomol. Chem.* 2013, **11**, 3177-3186.

14 S. P. Jones, N. P. Gabrielson, D. W. Pack and D. K. Smith, *Chem. Commun.* 2008, 4700-4702.

15 (*a*) D. J. Welsh, S. P. Jones and D. K. Smith, *Angew. Chem. Int. Ed.* 2009, **48**, 4047-4051. (*b*) A. Barnard, P. Posocco, S. Pricl, M. Calderon, R. Haag, M. E. Hwang, V. W. T. Shum, D. W. Pack and D. K. Smith, *J. Am. Chem. Soc.* 2011, **133**, 20288-20300.

16 (*a*) M. A. Kostiainen and H. Rosilo, *Chem. Eur. J.* 2009, **15**, 5656-5660. (*b*) A.-P. Eskelinen, H. Rosilo, A. Kuzyk, P. Torma and M. A. Kostiainen, *Small* 2012, **8**, 2016-2020.

17 For selected examples see: (*a*) P. Erbacher, J.-S. Remy and J.-P. Behr, *Gene Ther.* 1999, **6**, 138-145. (*b*) B. Wetzer, G. Byk, M. Frederic, M. Airiau, F. Blanche, B. Pitard and D. Scherman, *Biochem. J.* 2001, **356**, 747-756. (*c*) E. Dauty, J. S. Remy, T. Blessing and J.-P. Behr, *J. Am. Chem. Soc.* 2001, **123**, 9227-9234. (*d*) D. Oupický, A. L. Parker and L. W. Seymour, *J. Am. Chem. Soc.* 2002, **124**, 8-9. (*e*) K. Miyata, Y. Kakizawa, N. Nishiyama, A. Harada, Y. Yamasaki, H. Koyama and K. Kataoka, *J. Am. Chem. Soc.* 2004, **126**, 2355-2361. (*f*) G. T. Zugates, D. G. Anderson, S. R. Little, I. E. B. Lawhorn and R. Langer, *J. Am. Chem. Soc.* 2006, **128**, 12726-12734. (*g*) M. Breunig, U. Lungwitz, R. Liebl and A. Goepferich, *Proc. Natl. Acad. Sci. U.S.A.* 2007, **104**, 14454-14459. (*h*) S. Takae, K. Miyata, M. Oba, T. Ishii, N. Nishiyama, K. Itaka, Y. Yamasaki, H. Koyama and K. Kataoka, *J. Am. Chem. Soc.* 2008, **130**, 6001-6009. (*i*) K. Tanaka, T. Kanazawa, T. Ogawa, Y. Suda, Y. Takashima, T. Fukuda and H. Okada, *Chem. Pharm. Bull.* 2011, **59**, 202-207. (*j*) H. S. Hwang, H. C. Kang and Y. H. Bae, *Biomacromolecules* 2013, **14**, 548-556.

18 (*a*) M. Avital-Shmilovici and D. Shabat, *Soft Matter* 2010, **6**, 1073-1080. (*b*) A. D. Wong, M. A. DeWit and E. R. Gillies, *Adv. Drug Deliv. Rev.* 2012, **64**, 1031-1045.

19 (*a*) R. R. Ramireddy, K. R. Raghupathi, D. A. Torres and S. Thayumanavan, *New J. Chem.* 2012, **36**, 340-349. (*b*) S. V. Aathimanikandan, E. N. Savariar and S. Thayumanavan, *J. Am. Chem. Soc.* 2005, **127**, 14922-14929. (*c*) V. Yesilyurt, R. Ramireddy and S. Thayumanavan, *Angew. Chem. Int. Ed.* 2011, **50**, 3038-3042. (*d*) A. Almutairi, S. J. Guilladeu, M. Y. Berezin, S. Achilefu and S. Thayumanavan, *J. Am. Chem. Soc.* 2008, **130**, 444-445. (*e*) M. A. Azargasamy, P. Sokkalingam and S. Thayumanavan, *J. Am. Chem. Soc.* 2009, **131**, 14184-14185.

20 (*a*) H. Ihre, A. Hult, J. M. J. Fréchet and I. Gitsov, *Macromolecules* 1998, **31**, 4061-4068. (*b*) H. Ihre, O. L. Padilla de Jesus and J. M. J. Fréchet, *J. Am. Chem. Soc.* 2001, **123**, 5908-5917. (*c*) E. R. Gillies and J. M. J. Fréchet, *J. Am. Chem. Soc.* 2002, **124**, 14137-14146. (*d*) P. Wu, M. Malkoch, J. N. Hunt, R. Vestberg, E. Kaltgrad, M. J. Finn, V. V. Fokin, K. B. Sharpless and C. J. Hawker, *Chem. Commun.* 2005, 5775-5777.

21 L. Prokai, K. Prokai-Tatrai, X. Ouyang, H.-S. Kim, W.-M. Wu, A. Zharikova and N. Bodor, *J. Med. Chem.* 1999, **42**, 4563-4571.

22 M. C. A. Stuart, J. C. van de Pas and J. B. F. N. Engberts, *J. Phys. Org. Chem.* 2005, **18**, 929-934.

23 (*a*) B. F. Cain, B. C. Baguley and W. A. Denny, *J. Med. Chem.* **1978**, *21*, 658-668. (*b*) H. Gershon, R. Ghirlando, S. B. Guttman and A. Minsky, *Biochemistry* 1993, **32**, 7143-7151.

Cite this: DOI: 10.1039/c0xx00000x

www.rsc.org/xxxxxx

ARTICLE TYPE

Graphical Abstract

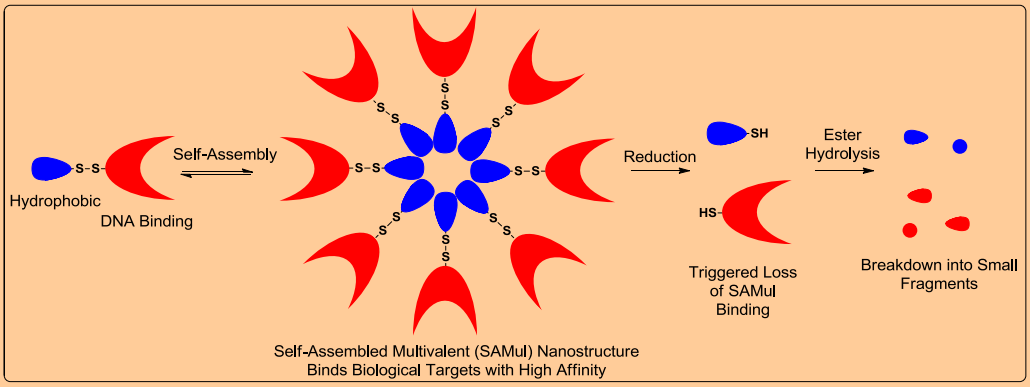

A two-step degradation mechanism allows self-assembled multivalency to be switched off, enabling nanostructures with capacity for high-affinity bio-intervention to be converted into small inactive fragments.